Harmonic Leakage and Image Quality Degradation in Tissue Harmonic Imaging

Che-Chou Shen and Pai-Chi Li, *Member, IEEE*

***Abstract*—Image quality degradation caused by harmonic leakage was studied for finite amplitude distortion-based harmonic imaging. Various sources of harmonic leakage, including transmit waveform, signal bandwidth, and system nonlinearity, were investigated using both simulations and hydrophone measurements. Effects of harmonic leakage in the presence of sound velocity inhomogeneities were also considered. Results indicated that sidelobe levels of the harmonic beam pattern were directly affected by harmonic leakage when the harmonic signal was obtained by filtering out the fundamental signal. Because sidelobe levels also increase with the bandwidth of the transmitted signal, a trade-off exists between axial resolution and contrast resolution. It is concluded that accurate control of the frequency content of the waveform prior to propagation is necessary to optimize imaging performance of tissue harmonic imaging. The filtering technique was also compared with the pulse inversion technique. It was shown that the pulse inversion technique effectively suppresses harmonic leakage at the cost of imaging frame rate and potential motion artifacts.**

I. Introduction

Finite amplitude distortion-based harmonic imaging has been proven to provide superior image resolution compared with conventional fundamental imaging [1]–[4]. Such an imaging method is also known as tissue harmonic imaging. Simulations, experiments, and clinical evaluations have been performed by various research groups to study the benefits of tissue harmonic imaging. Christopher performed both simulations and experiments to study beamforming characteristics of a finite amplitude propagating beam [1], [2]. It was found that sidelobes of the nonlinearly generated beam are much lower than those of the linear beam. Such an advantage also exists in the presence of tissue inhomogeneities. Therefore, tissue harmonic imaging generally has better contrast resolution than fundamental imaging. One disadvantage of tissue harmonic imaging is the low harmonic amplitude. Li and Shen suggested that dynamic transmit focusing may be employed to increase finite amplitude distortion-based harmonic generation and to improve sensitivity and penetration of tissue harmonic imaging [3]. Clinical benefits of tissue harmonic imaging have also been demonstrated by Tranquart *et al.* [4]. Results of this study showed that tissue harmonic imaging provides clinically important information that may be absent from linear imaging. These clinical findings were also consistent with previous simulations and experimental results.

The tissue harmonic signal is generated by nonlinearity of the propagating medium. Because the propagation velocity increases with the instantaneous acoustic pressure, the acoustic waveform is distorted during propagation, and, thus, harmonics are generated [5]–[7]. On the other hand, harmonic signals may be generated by the imaging system itself. Such signals are independent of the nonlinear characteristics of the propagating medium. In other words, the harmonic signal present at a particular imaging depth consists of two components. One is the tissue harmonic signal generated through finite amplitude propagation; the other is the harmonic leakage signal produced by the imaging system prior to acoustic propagation. The leakage signal produces acoustic beams with different characteristics and may significantly affect image quality. It is the primary purpose of this paper to investigate effects of harmonic leakage on image quality under various imaging conditions.

A typical ultrasound transmitter has three main components: a waveform generator, a high voltage amplifier with a transmit/receive switch, and a transducer. A transmit waveform is produced by the waveform generator and amplified by the high voltage amplifier. The transducer converts the electrical signal and sends out an acoustic pulse. Several sources of harmonic signals may be introduced in the transmitter. First, the signal produced by the waveform generator may have frequency components outside of the fundamental bandwidth. The amount of leakage is directly related to characteristics of the transmit waveform. In general, envelopes with a smooth shape (e.g., Gaussian envelopes) have lower harmonic amplitudes than envelopes with sharp edges (e.g., square envelopes). A wide fundamental bandwidth may also produce harmonic leakage because it may have significant overlap with the harmonic bandwidth. Second, harmonic leakage may also result from the waveform distortion produced by high voltage amplification and transmit/receive switching. Finally, the transducer may further distort the waveform during the electro-mechanical conversion. It is apparent that non-negligible harmonic components may have been present at the surface of the transducer prior to acoustic propagation. At a particular imaging depth, linear propagation of such a leakage signal is combined with the finite amplitude distortion-based harmonic signal. Because these two

Manuscript received March 27, 2000; accepted December 19, 2000. Support supplied from the National Science Council of R.O.C. under Grant NSC 89-2320-B-002-152-M08 is gratefully acknowledged.

The authors are with the Department of Electrical Engineering, National Taiwan University, Taipei, Taiwan, R.O.C. (e-mail: paichi@cc.ee.ntu.edu.tw).

signals have the same frequency range, the leakage signal cannot be filtered out and may significantly affect the tissue harmonic signal.

Effects of harmonic leakage have been discussed for contrast agent-based harmonic imaging. When the contrast agents are insonified near its resonance frequency, the backscattered signal produced by the agents at the second harmonic frequency is several orders of magnitude stronger than the corresponding tissue harmonic signal. However, the contrast may be reduced in the presence of harmonic leakage. Several approaches were proposed, and efficacy of leakage suppression was demonstrated [8].

Effects of harmonic leakage in tissue harmonic imaging are investigated in this paper using both simulations and experiments. In Section II, three typical transmit waveforms, including the Gaussian pulse, the gated sine wave, and the gated square wave, are considered. Gaussian pulses with various bandwidths are also evaluated. It is shown that harmonic leakage significantly affects beam characteristics and a trade-off between contrast resolution and axial resolution exists. In Section III, effects of harmonic leakage in the presence of tissue inhomogeneities are studied. Similar degradation caused by harmonic leakage is demonstrated. Results from hydrophone measurements are shown in Section IV to illustrate the harmonic leakage effects caused by system nonlinearity and signal bandwidth. The paper concludes in Section V with a discussion on harmonic leakage suppression using the pulse inversion technique.

II. Transmit Waveforms and Harmonic Beam Patterns

Effects of various transmit waveforms on harmonic beam patterns were studied using simulations. The simulation model used is similar to the one used by Christopher [1] and Li and Shen [3]. The model approximates continuous beam formation by incremental field propagation, and acoustic propagation of arbitrary transmit waveforms can be simulated. The waveform is first decomposed into discrete temporal frequency components. At each increment, linear propagation is simulated based on the angular spectrum method [9], [10]. The nonlinear propagation is done based on a finite amplitude distortion model [11]. As shown in the following equation, the finite amplitude distortion model utilizes the frequency domain solution to Burgers' equation, i.e.,

$$u_n(z+\Delta z,i) = u'_n(z+\Delta z,i) + j\frac{\beta\pi f\Delta z}{2c^2}\left(\sum_{k=1}^{n-1} k u'_k u'_{n-k} + \sum_{k=n}^{N} n u'_k u'^{*}_{k-n}\right). \quad (1)$$

In (1), z is the propagation direction, and Δz is the propagation increment. The fundamental frequency is denoted by f, and β is a parameter representing the nonlinearity of the propagating medium. The term $u'_n(z+\Delta z,i)$ denotes the temporal velocity field at frequency nf (n is an integer) and at depth $z+\Delta z$ after linear propagation. $u_n(z+\Delta z,i)$ denotes the temporal velocity field after nonlinear propagation. The symbol c is the sound velocity. It is clearly shown in (1) that the harmonic signal consists of two components. One is the previously generated harmonic signal via linear propagation; the other is the newly generated harmonic signal caused by finite amplitude distortion. Therefore, linear propagation of the leakage signal directly affects the harmonic signal produced by finite amplitude distortion.

Simulation results shown in this paper assumed a one-dimensional, 96-channel linear array. The array had a 0.25-mm pitch, and the transmit focus was set to 55 mm, away from the transducer. The propagating medium was homogeneous, and the nonlinear parameter β was set to 3.5, approximating the nonlinear property of water [12]. Frequency response of the transducer is Gaussian with a 3-MHz center frequency and 80% fractional bandwidth (−6 dB). After nonlinear propagation, the signal was divided into a fundamental band and a harmonic band. The fundamental signal was extracted by low-pass filtering with a flat frequency response between dc and 3 MHz. The harmonic signal was extracted by band pass filtering with a flat frequency response between 3 and 6 MHz.

Three types of transmit waveforms were investigated. They were the Gaussian pulse, the gated sine wave, and the gated square wave. Both the gated sine wave and the gated square wave had envelopes with uniform amplitude. The bandwidth of such waveforms is inversely proportional to the time duration. On the other hand, the Gaussian pulse had a non-uniform envelope, and generation of such transmit waveforms is relatively complicated. Typically, a digital waveform buffer and a digital-to-analog converter are required.

Fig. 1 shows the three transmit waveforms in the upper panel. The lower panel shows spectra of the convolution of the three transmit waveforms with the transducer's frequency response. For all three waveforms, the center frequency was 2 MHz with a −6 dB 25% fractional bandwidth. In both panels, the dashed line represents the Gaussian pulse, the solid line denotes the gated sine wave, and the dotted line is for the gated square wave. As observed in the spectra, the gated sine wave and the gated square wave had significantly higher harmonic amplitudes primarily because of the shape of the envelopes.

To demonstrate potential image quality degradation caused by harmonic leakage, two focal plane beam patterns are shown in Fig. 2. The solid line represents a linear beam produced by a Gaussian pulse with a 4-MHz center frequency. The dotted line denotes a second harmonic beam produced by a Gaussian pulse with a fundamental frequency at 2 MHz. The fractional bandwidth of the 2-MHz Gaussian pulse was 25%. The bandwidth of the 4-MHz pulse was chosen such that it was the same as the second harmonic bandwidth of the nonlinear response of the 2-MHz Gaussian pulse. It is shown that the linear beam has much higher sidelobes than the nonlinear beam. By using a filter to extract the harmonic signal, the har-

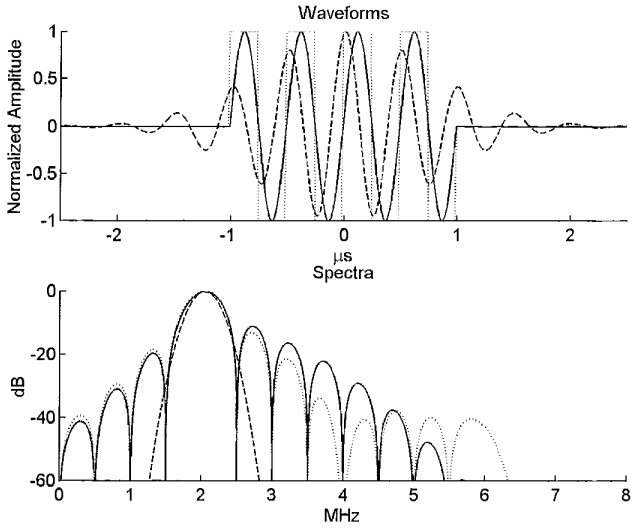

Fig. 1. Waveforms (upper panel) and spectra (lower panel) of Gaussian pulse (dashed line), gated sine wave (solid line), and gated square wave (dotted line). Center frequency is 2 MHz, and fractional bandwidth is 25%.

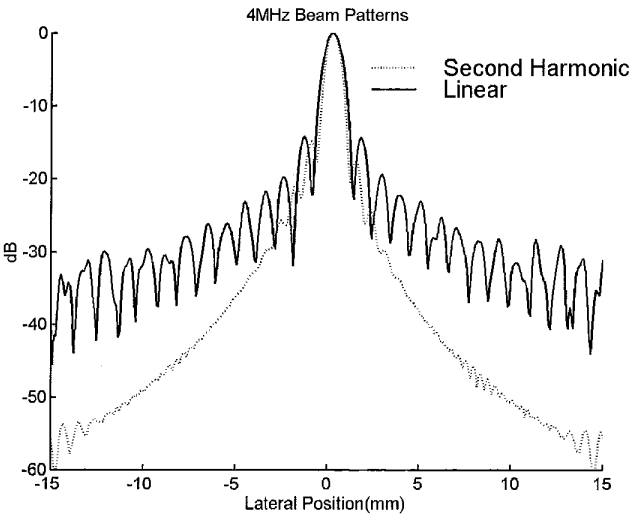

Fig. 2. Simulated 4-MHz harmonic beam pattern (dotted line) and 4-MHz linear beam pattern (solid line).

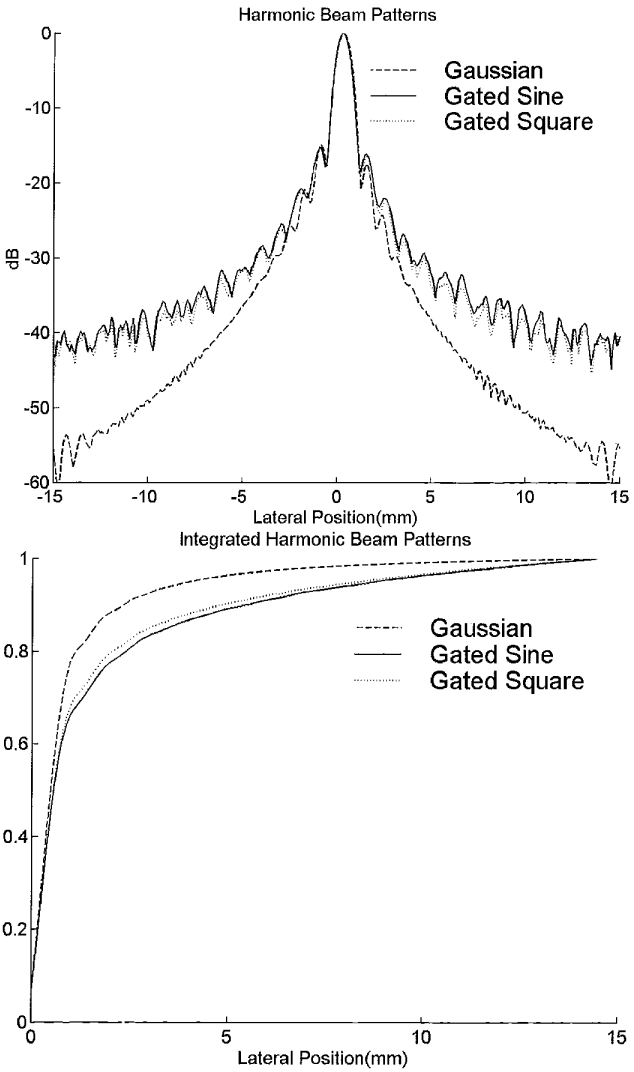

Fig. 3. Simulated harmonic beam patterns (top) and normalized integrated harmonic patterns (bottom) of Gaussian pulse (dashed line), gated sine wave (solid line), and gated square wave (dotted line). Fractional bandwidth is 25%.

monic beam becomes a combination of the linear beam (solid line) and the finite amplitude distorted harmonic beam (dotted line). Based on the comparison, it is clear that sidelobes of the second harmonic beam are elevated in the presence of harmonic leakage.

Simulated harmonic beam patterns of various transmit waveforms at the transmit focus are shown in the top panel of Fig. 3. The bottom panel of Fig. 3 shows the normalized, lateral integration of the intensity of the harmonic beam patterns shown in the top panel. The integration started from the center of the propagation axis and ended at a prespecified lateral position, 15 mm away from the beam center. Using such a representation, a profile that rises rapidly to unity represents low sidelobe levels and, hence, better contrast resolution. Fig. 3 demonstrates clearly that the Gaussian envelope produced significantly lower sidelobes. The two square waves had sidelobe levels similar to each other. Because of the similarity, only results of gated sine waveforms will be shown in the rest of this paper.

Fig. 3 showed effects of harmonic leakage for various types of transmit waveforms with the same bandwidth. For a given type of waveform, the bandwidth also affects the amount of harmonic leakage. Fig. 4 shows the output spectra of two Gaussian pulses. One had a 25% fractional bandwidth, and the other had a 50% fractional bandwidth. As the bandwidth increases, the high frequency portion of the transmit signal enters the second harmonic bandwidth, thus causing harmonic leakage. Note that the shift in center frequency of the 50% spectrum is due to the fact that

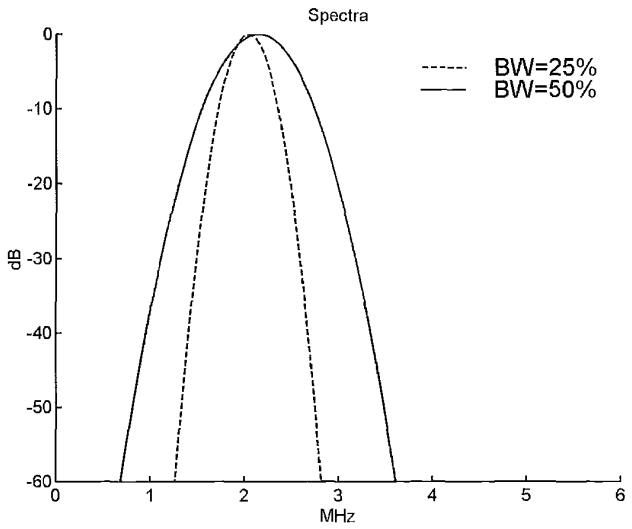

Fig. 4. Output spectra of Gaussian pulses with 25% (dashed line) and 50% (solid line) fractional bandwidths.

the center frequency of the transmit waveform is lower than the center frequency of the transducer. A relatively low transmit center frequency is typically used so that the received second harmonic signal is still within the transducer's passband.

Harmonic beam patterns associated with the two bandwidths are demonstrated in Fig. 5. Similar to Fig. 3, the top panel of Fig. 5 shows the harmonic beam patterns, and the bottom panel shows the normalized, laterally integrated beam patterns. It is demonstrated that the smaller bandwidth had less harmonic leakage and, thus, produces lower sidelobes. Although a smaller bandwidth provides lower sidelobes and better contrast resolution, one drawback is the degraded axial resolution. In other words, a trade-off exists between axial resolution and contrast resolution.

A large bandwidth is often used in B-mode imaging to improve axial resolution. Fig. 6 compares beam patterns of the waveforms with a 50% fractional bandwidth. The display format of Fig. 6 is the same as that of Fig. 3. In addition, a 4-MHz linear beam pattern is also presented as the dot-dashed line for comparisons. Because of the increased bandwidth, the leakage increases significantly compared with the previous cases with a 25% fractional bandwidth. The harmonic beam patterns shown in the top panel of Fig. 6 indicate that differences in sidelobe levels between various waveforms become smaller as the bandwidth increases. In other words, the benefits of Gaussian type waveforms are less significant if a large bandwidth is used for improved axial resolution. Nevertheless, these nonlinearly generated beam patterns still have lower sidelobes than those of the 4-MHz linear beam. Thus, improved contrast of tissue harmonic imaging is still expected.

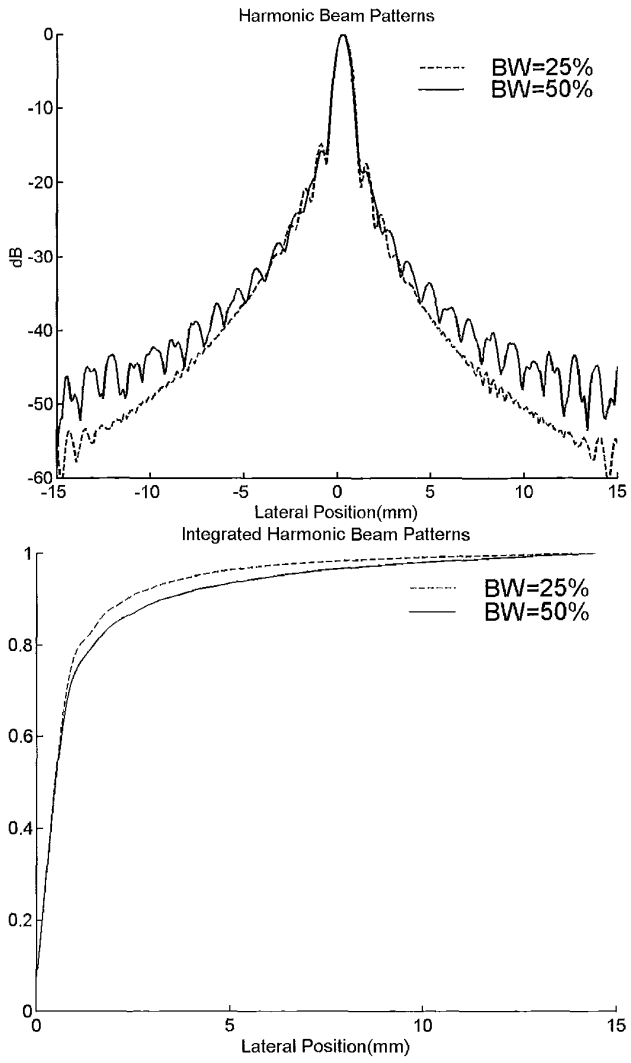

Fig. 5. Simulated harmonic beam patterns (top) and normalized integrated harmonic patterns (bottom) of Gaussian pulses with 25% (dashed line) and 50% (solid line) fractional bandwidths.

III. Effects of Harmonic Leakage in Inhomogeneous Tissue

Previous simulations assumed a homogeneous propagating medium. In most clinical applications, however, the ultrasound beam passes through various tissues with different acoustic characteristics. Particularly, the sound velocity variations may significantly distort acoustic beams and degrade image quality. Extensive research works have been conducted in this area [13]–[20]. In tissue harmonic imaging, it has also been shown that acoustic beams are less affected by sound velocity inhomogeneities [1]. In this section, we will extend the previous work and use an example to illustrate effects of harmonic leakage in an inhomogeneous medium.

A displaced phase screen was included in the simulations to model sound velocity variations. Such a model

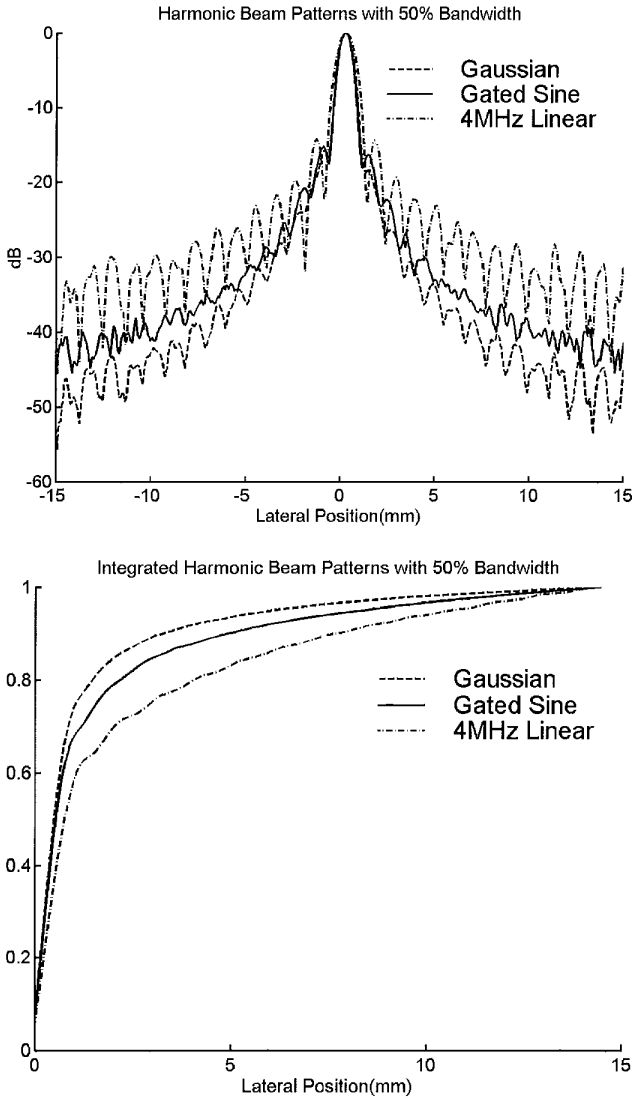

Fig. 6. Simulated harmonic beam patterns (top) and normalized integrated harmonic patterns (bottom) of Gaussian pulse (dashed line), gated sine wave (solid line), and 4-MHz linear beam (dot-dashed line). Fractional bandwidth is 50%.

is similar to the one proposed by Liu and Waag [15]. Two different media were included in the simulations. The medium next to the transducer had a propagation velocity of 1.45 mm/μs, a uniform thickness of 15 mm, and a β of 6 to mimic the nonlinear properties of fat tissue [12]. The deeper medium had a propagation velocity of 1.54 mm/μs, a thickness of 65 mm, and a β of 3.5. The focus was set 55 mm away from transducer. Time delay errors resulting from irregular thickness of fat tissue were simulated using a two-dimensional phase screen at the boundary of the two media. The time delay errors had a correlation length of 5 mm, and the maximum of the absolute value of the time delay errors was 30 ns. Gray level image of the phase pattern is shown in Fig. 7 with a dynamic range from -30 to $+30$ ns.

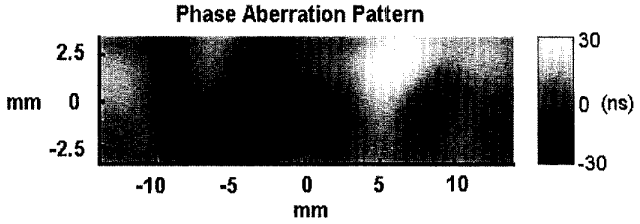

Fig. 7. The phase screen pattern. Positive phase shift is displayed in white, and the negative shift is in black. Maximum of the absolute value of the time error is 30 ns, and the correlation length is 5 mm.

Beam patterns produced by the Gaussian pulse and the gated sine wave were simulated with sound velocity inhomogeneities. The center frequency was again 2 MHz, and the fractional bandwidth was 25%. A 4-MHz linear beam was also included for comparison. Results are shown in Fig. 8. Compared with Fig. 3 (i.e., the same center frequency and bandwidth but without tissue inhomogeneities), it is observed that differences in sidelobe levels between the Gaussian pulse and the gated waves decreased. In other words, although the Gaussian pulse still provides the lowest sidelobes, the tissue inhomogeneities offset a portion of contrast resolution improvement provided by the Gaussian pulse. Nevertheless, contrast improvement over linear imaging at the same frequency is still evident.

IV. Experimental Results

Hydrophone measurements were done to investigate experimentally the harmonic leakage effects. A schematic diagram of the experimental set-up is shown in Fig. 9. An arbitrary function generator (Hewlett-Packard E1445A, Palo Alto, CA) was used to generate the desired transmit waveform. The transmit waveform was then sent to a power amplifier (Amplifier Research 25A250A, Souderton, PA) to drive a 3.5-MHz focused transducer (Panametrics V381, Waltham, MA). The transducer had a diameter of 19 mm and was geometrically focused at 70 mm.

Acoustic beam patterns in water were measured by a PVDF needle hydrophone with a 30-dB pre-amplifier gain (NTR Systems TNU001A, Seattle, WA). The hydrophone had a diameter of 0.6 mm with a flat frequency response from 1 to 20 MHz. Position of the hydrophone was controlled by a three-axis step motor system with a 5-μm step size (Q-Sync, Hsine-Chu, Taiwan, R.O.C.). The signal was sent to an ultrasonic receiver (Panametrics Model 5900, Waltham, MA) for further amplification to match dynamic range of the analog-to-digital converter. The analog-to-digital converter had a 20-Msamples sampling rate with 12-bit resolution (Hewlett-Packard E1429A, Palo Alto, CA). The arbitrary function generator and the analog-to-digital converter were both VXI modules housed in a VXI mainframe (Hewlett-Packard E1401B, Palo Alto, CA). The whole system was controlled by a Pentium-class personal computer with HP VEE software.

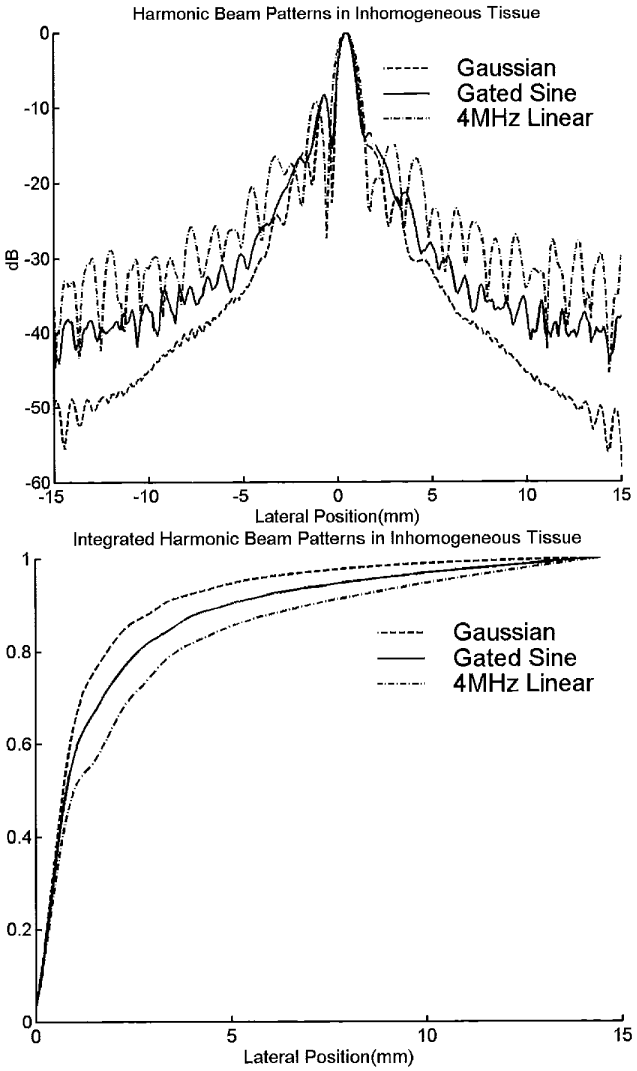

Fig. 8. Simulated harmonic beam patterns (top) and normalized integrated harmonic patterns (bottom) of Gaussian pulse (dashed line), gated sine wave (solid line), and 4-MHz linear beam (dot-dashed line). Tissue inhomogeneities are included. Fractional bandwidth is 25%.

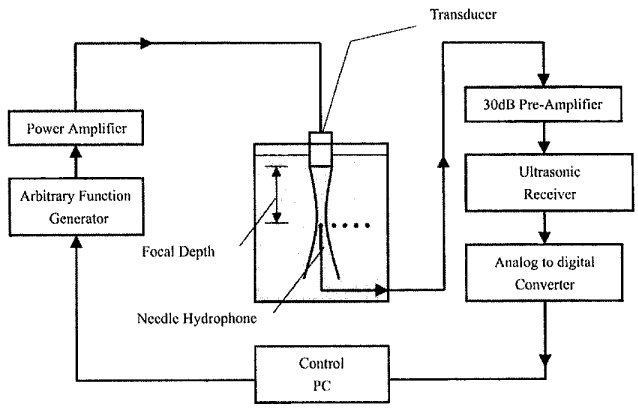

Fig. 9. Schematic diagram of the hydrophone measurement set-up.

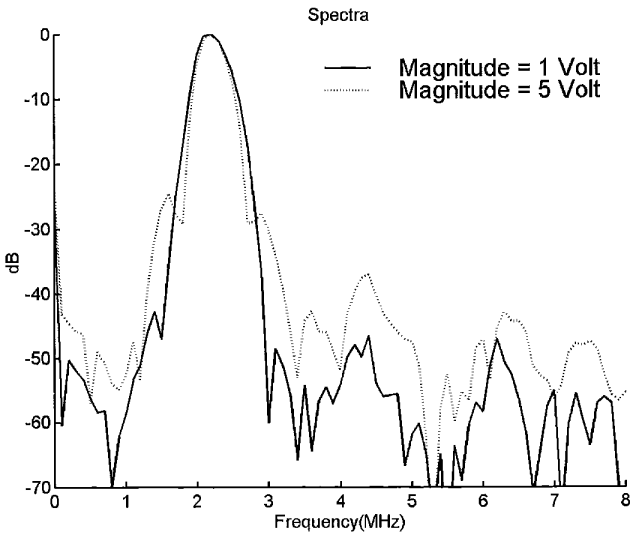

Fig. 10. Measured spectra near the transducer surface. The dotted line is with the 5-V peak amplitude, and the solid is with the 1-V peak amplitude.

Acoustic beam patterns were sampled in the focal plane with a spacing of 0.1 mm. Because the transducer was circularly symmetric, acoustic beams generated by the transducer were also circularly symmetric. Therefore, only one-dimensional, lateral measurements were performed. At each measurement point, the acoustic field was measured 1000 times for off-line signal averaging. To avoid misalignment of beam patterns caused by stepping errors, the hydrophone was moved to a new position after acoustic fields produced by all transmit waveforms had been measured.

The simulations in the previous sections ignored system nonlinearity. In other words, both the transmitter and the transducer were assumed purely linear so that no additional harmonics were generated before acoustic propagation. In practice, system nonlinearity must not be ignored. To assess potential effects, two Gaussian pulses with different amplitudes were evaluated. Both waveforms had a 2.25-MHz center frequency and a 25% fractional bandwidth. The only difference between the two waveforms was that one had a 1-V peak amplitude and the other had a 5-V peak amplitude at the output of the arbitrary function generator. After amplification, the actual driving voltage was approximately 20 times higher than the output voltage of the function generator. It was expected that the 5-V waveform should be more affected by system nonlinearity.

Spectra of the acoustic signal received near the transducer surface are shown in Fig. 10. The solid line represents the spectrum of the 1-V Gaussian pulse and the dotted line represents the 5-V spectrum. Because a 25% bandwidth Gaussian pulse has negligible overlap between the fundamental and the second harmonic bandwidths, it is assumed that harmonics near the transducer surface mainly resulted from the system nonlinearity. As the signal amplitude increased, peak harmonic levels also increased roughly from -50 to -40 dB.

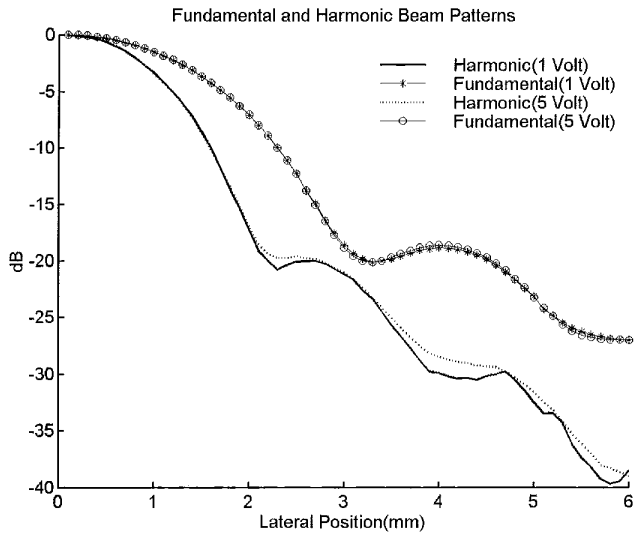

Fig. 11. Measured fundamental and harmonic beam patterns in the focal plane. The dotted line corresponds to the 5-V harmonic pattern, and the solid line corresponds to the 1-V harmonic pattern. The solid line with asterisks denotes the 1-V fundamental pattern, and the solid line with circles denotes the 5-V fundamental pattern.

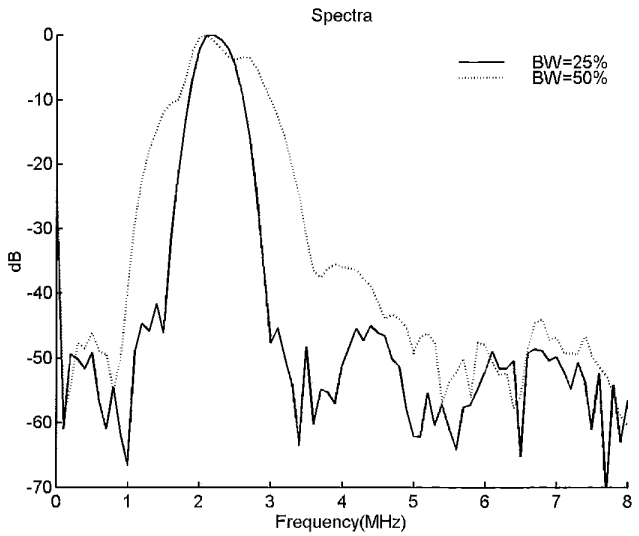

Fig. 12. Measured spectra near transducer surface. 25% bandwidth Gaussian (solid line) and 50% bandwidth Gaussian (dotted line) are shown.

Focal plane beam patterns of the above two cases are shown in Fig. 11. The solid line with asterisks represents the fundamental beam pattern of the 1-V waveform, and the solid line with circles represents that of the 5-V waveform. The two fundamental beam patterns are very similar to each other. That is, the system nonlinearity has negligible influence on linear imaging in this case. Although the peak harmonic levels of the two waveforms were low (−50 to −40 dB relative to the peak of the fundamental signal), the harmonic beam patterns are noticeably different. It is shown that the 5-V waveform (denoted by the dotted line) produced sidelobes consistently higher than did the 1-V waveform (denoted by the solid line). As system nonlinearity increases, it is expected that effects of harmonic leakage will be more apparent. Potential contrast degradation caused by system nonlinearity is clearly demonstrated.

In addition to system nonlinearity, effects of the signal bandwidth were also experimentally investigated. Two Gaussian pulses were used. The center frequency was 2.25 MHz for both waveforms. Bandwidths of the two waveforms were 25 and 50%. A 1-V peak amplitude of the output of the arbitrary function generator was used. Note that higher voltages were not chosen to avoid introducing additional system nonlinearity. Spectra and beam patterns are demonstrated in Fig. 12 and 13, respectively. The solid line represents the 25% case, and the dotted line denotes the 50% case in both figures. Note that the spectra were measured near the transducer surface, and the beam patterns were measured at focus. As the bandwidth increased, sidelobes were also elevated. As shown in Fig. 12, the 25% case had harmonic components introduced by system nonlinearity. This reduces the differences in sidelobe level between the two bandwidths.

Except for the harmonics introduced by system nonlinearity, the experimental results are consistent with previous simulations.

V. Concluding Remarks

Potential degradation in contrast resolution caused by harmonic leakage was investigated using both simulations and hydrophone measurements. Simulation results based on various transmit waveforms and bandwidths showed that contrast resolution in tissue harmonic imaging is directly affected by harmonic leakage. The trade-off between contrast resolution and axial resolution was also noted. It was shown that transmit waveform, signal bandwidth, and system nonlinearity may all introduce harmonic leakage and degrade contrast resolution with or without sound velocity inhomogeneities. In addition, the improvement caused by a smooth envelope (which requires a more sophisticated transmitter) becomes marginal if a large bandwidth is used or tissue inhomogeneities are present. The results in this paper help to understand performance issues in tissue harmonic imaging better.

To take full advantage of tissue harmonic imaging, harmonic leakage needs to be minimized. Imaging methods that can suppress the leakage effects are of particular interest. One example is the alternative phasing technique proposed by Krishnan and O'Donnell [8]. However, efficacy of such methods must be evaluated based on the ability of leakage suppression and potential deterioration of the fundamental beam. Because the finite amplitude distortion-based harmonic beam is produced by nonlinear propagation of the fundamental beam, it is apparent that a high quality fundamental beam is necessary to produce a high quality harmonic beam.

Instead of filtering, another potential solution is to use the pulse inversion technique [21], [22]. Simulation results

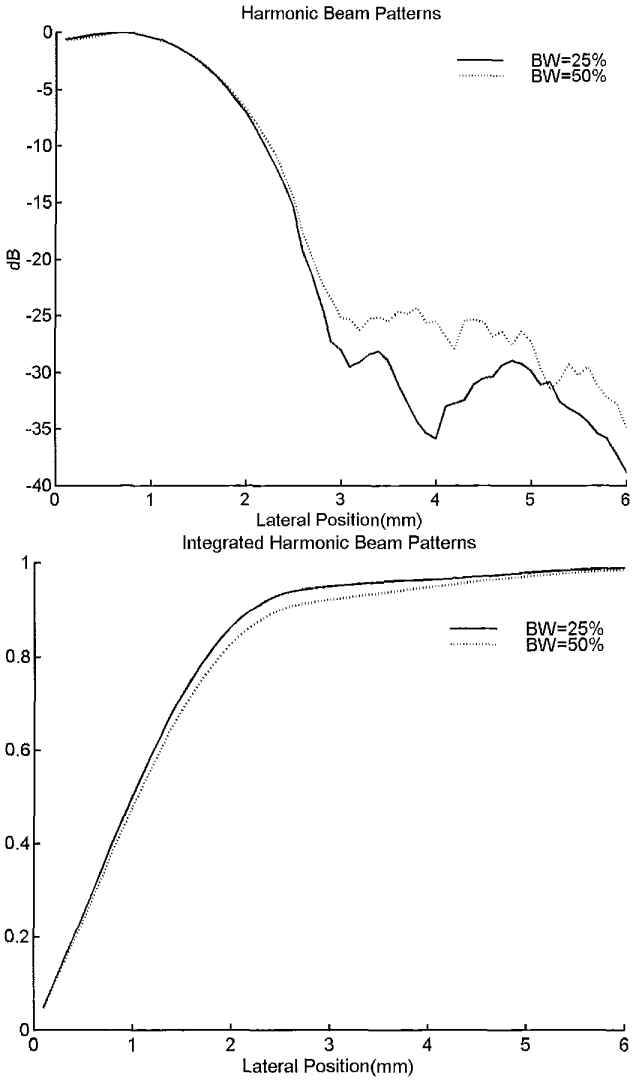

Fig. 13. Measured harmonic beam patterns in the focal plane (top) and normalized integrated harmonic patterns (bottom). The solid line corresponds to a 25% bandwidth. The dotted line corresponds to a 50% bandwidth.

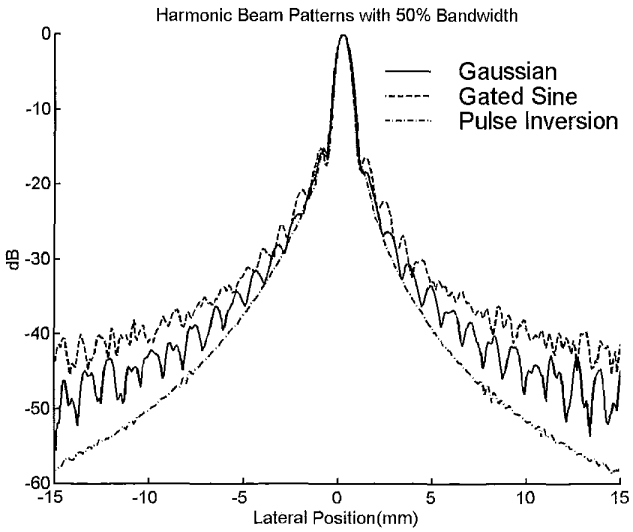

Fig. 14. Simulated harmonic beam patterns of Gaussian pulse (solid line), gated sine wave (dashed line), and gated sine wave with the pulse inversion technique (dot-dashed line). Fractional bandwidth is 50%.

are shown in Fig. 14. Harmonic beams for 50% Gaussian with filtering (solid), 50% gated sine with filtering (dashed), and 50% gated sine with pulse inversion technique (dot-dashed) are shown.

The pulse inversion method effectively removes effects of harmonic leakage and produces the lowest sidelobes. Although the pulse inversion technique is very effective, it suffers from frame rate reduction and potential motion artifacts. Development of alternative methods for harmonic leakage suppression is the focus of current research.

Acknowledgments

The authors would like to thank the reviewers for helpful comments.

References

[1] T. Christopher, "Finite amplitude distortion-based inhomogeneous pulse echo ultrasonic imaging," *IEEE Trans. Ultrason., Ferroelect., Freq. Contr.*, vol. 44, no. 1, pp. 125–139, Jan. 1997.

[2] ——, "Experimental investigation of finite amplitude distortion-based second harmonic pulse echo ultrasonic imaging," *IEEE Trans. Ultrason., Ferroelect., Freq. Contr.*, vol. 45, no. 1, pp. 158–162, Jan. 1998.

[3] P. C. Li and C. C. Shen, "Effects of transmit focusing on finite amplitude distortion based second harmonic generation," *Ultrason. Imaging*, vol. 21, no. 4, pp. 243–258, 1999.

[4] F. Tranquart, N. Grenier, V. Eder, and L. Pourcelot, "Clinical use of ultrasound tissue harmonic imaging," *Ultrasound Med. Biol.*, vol. 25, no. 6, pp. 889–894, 1999.

[5] C. A. Cain, "Ultrasonic reflection mode imaging of the nonlinear parameter B/A: I. A theoretical basis," *J. Acoust. Soc. Amer.*, vol. 80, no. 1, pp. 28–32, Jul. 1986.

[6] R. T. Beyer and S. V. Letcher, *Nonlinear Acoustics*. New York: Academic, 1969, pp. 202–230, ch. 7.

[7] M. E. Haran and B. D. Cook, "Distortion of finite amplitude ultrasound in lossy media," *J. Acoust. Soc. Amer.*, vol. 73, no. 3, no. 2, pp. 774–779, Mar. 1983.

[8] S. Krishnan and M. O'Donnell, "Transmit aperture processing for non-linear contrast agent imaging," *Ultrason. Imaging*, vol. 18, no. 2, pp. 77–105, 1996.

[9] D. L. Liu and R. C. Waag, "Propagation and backpropagation for ultrasonic wavefront design," *IEEE Trans. Ultrason., Ferroelect., Freq. Contr.*, vol. 44, no. 1, pp. 1–12, Jan. 1997.

[10] J. W. Goodman, *Introduction to Fourier Optics*. New York: McGraw-Hill, 1968.

[11] P. T. Christopher and K. J. Parker, "New approaches to nonlinear diffractive field propagation," *J. Acoust. Soc. Amer.*, vol. 90, no. 1, pp. 488–499, Jul. 1991.

[12] W. K. Law, L. A. Frizzell, and F. Dunn, "Determination of the nonlinearity parameter B/A of biological media," *Ultrasound Med. Biol.*, vol. 11, no. 2, pp. 307–318, 1985.

[13] S. W. Flax and M. O'Donnell, "Phase-aberration correction using signals from point reflectors and diffuse scatterers: Basic principles," *IEEE Trans. Ultrason., Ferroelect., Freq. Contr.*, vol. 35, no. 6, pp. 758–767, Nov. 1988.

[14] M. O'Donnell and S. W. Flax, "Phase-aberration correction using signals from point reflectors and diffuse scatterers: Measurements," *IEEE Trans. Ultrason., Ferroelect., Freq. Contr.*, vol. 35, no. 6, pp. 768–774, Nov. 1988.

[15] D. L. Liu and R. C. Waag, "Correction of ultrasonic wavefront distortion using backpropagation and a reference waveform method for time-shift compensation," *J. Acoust. Soc. Amer.*, vol. 96, no. 2, pp. 649–659, Aug. 1994.
[16] L. M. Hinkelman and D. L. Liu, "Measurement and correction of ultrasonic pulse distortion produced by human breast," *J. Acoust. Soc. Amer.*, vol. 97, no. 3, pp. 1958–1969, Mar. 1995.
[17] L. M. Hinkelman, L. A. Metlay, and R. C. Waag, "Measurement of ultrasonic pulse arrival time and energy level variations produced by propagation through abdominal wall," *J. Acoust. Soc. Amer.*, vol. 95, no. 1, pp. 530–541, Jan. 1994.
[18] G. C. Ng, P. D. Freiburger, W. F. Walker, and G. E. Trahey, "A speckle target adaptive imaging technique in the presence of distributed aberrations," *IEEE Trans. Ultrason., Ferroelect., Freq. Contr.*, vol. 44, no. 1, pp. 140–151, Jan. 1997.
[19] P. C. Li and M. O'Donnell, "Phase aberration correction on two-dimensional conformal arrays," *IEEE Trans. Ultrason., Ferroelect., Freq. Contr.*, vol. 42, no. 1, pp. 73–82, Jan. 1995.
[20] S. Krishnan, K. W. Rigby, and M. O'Donnell, "Improved estimation of phase aberration profile," *IEEE Trans. Ultrason., Ferroelect., Freq. Contr.*, vol. 44, no. 3, pp. 701–713, May 1997.
[21] D. H. Simpson and P. N. Burns, "Pulse inversion doppler: A new method for detecting nonlinear echoes from microbubble contrast agents," in *Proc. IEEE Ultrason. Symp.*, pp. 1597–1600, 1997.
[22] D. H. Simpson, C. T. Chin, and P. N. Burns, "Pulse inversion doppler: A new method for detecting nonlinear echoes from microbubble contrast agents," *IEEE Trans. Ultrason., Ferroelect., Freq. Contr.*, vol. 46, no. 2, pp. 372–382, Mar. 1999.

Che-Chou Shen was born in 1976 in Taiwan, R.O.C. He graduated from the Department of Electrical Engineering at National Taiwan University in 1998. He is now a graduate student working on ultrasonic harmonic imaging under the instruction of Professor P.-C. Li.

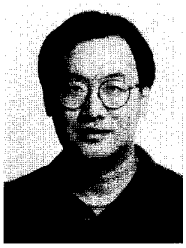

Pai-Chi Li (S'91–M'93–S'93–M'95) received the B.S. degree in electrical engineering from National Taiwan University, Taipei, Taiwan, R.O.C. in 1987 and the M.S. and Ph.D. degrees from the University of Michigan, Ann Arbor in 1990 and 1994, respectively, both in electrical engineering: systems.

He was Research Assistant in the Department of Electrical Engineering and Computer Science from 1990 to 1994. He joined Acuson Corporation (Mountain View, CA) as a member of the Technical Staff in June 1994. His work in Acuson was primarily in the areas of medical ultrasonic imaging system design for both cardiology and general imaging applications. In August 1997, he went back to the Department of Electrical Engineering at National Taiwan University as Assistant Professor. He then became Associate Professor in August 1998. His current research interests include biomedical ultrasonic imaging and signal processing.

Dr. Li is a member of IEEE, and he was the recipient of the Distinguished Achievement Award in Electrical Engineering: Systems for his outstanding academic achievement at the University of Michigan.